Journal of Fluids and Structures 54 (2015) 122–141

Contents lists available at ScienceDirect

Journal of Fluids and Structures

journal homepage: www.elsevier.com/locate/jfs

Flow around circular cylinders with very low aspect ratio

R.T. Gonçalves [a,*], G.R. Franzini [b], G.F. Rosetti [a], J.R. Meneghini [b], A.L.C. Fujarra [a]

[a] TPN, Department of Naval Architecture and Ocean Engineering, Escola Politécnica, University of São Paulo, Av. Prof. Mello Moraes, 2231, Cidade Universitária, São Paulo, SP 05508-030, Brazil

[b] NDF, Department of Mechanical Engineering, Escola Politécnica, University of São Paulo, Av. Prof. Mello Moraes, 2231, Cidade Universitária, São Paulo, SP 05508-030, Brazil

ARTICLE INFO

Article history:
Received 3 October 2013
Accepted 2 November 2014
Available online 26 November 2014

Keywords:
Low aspect ratio cylinder
Flow around cylinder
Free-end effects

ABSTARCT

Experiments on the flow around stationary circular cylinders with very low aspect ratio piercing the water free surface were carried out in a recirculating water channel. Eight different aspect ratios were tested, namely $L/D=$ 0.1, 0.2, 0.3, 0.5, 0.75, 1.0, 1.5 and 2.0; no end-plates were employed. Forces were measured using a six degree-of-freedom load cell and the Strouhal number was inferred through the transverse force fluctuation frequency. The range of Reynolds number covered $10\,000 < \mathrm{Re} < 50\,000$. PIV measurements were performed in some aspect ratio cases, namely $L/D=$ 0.3, 0.5, 1.0 and 2.0 for Reynolds number equal to 43 000. The results showed a decrease in drag force coefficients with decreasing aspect ratio, as well as a decrease in Strouhal number with decreasing aspect ratio. The PIV measurements and the PSD of forces showed different behavior for cylinders with $L/D \leq 0.5$, in which cases the free-end effects were predominant. Even without von Kármán street main characteristics around the majority length of the cylinder, in the range of $0.2 < L/D \leq 0.5$, the vortex shedding around it is capable of producing alternating forces in the transverse direction. Therefore, alternating forces were not observed in the transverse direction for cylinders with $L/D \leq 0.2$.

1. Introduction

The flow field around stationary low aspect ratio cylinders, $L/D < 6$, where L is the immersed length of the cylinder and D is the diameter, is much less understood than the classical case of infinite length cylinder, in which the flow can be assumed as two-dimensional in most cases. Most publications on this subject refer to flow around surface-mounted low aspect ratio cylinders, in that the three-dimensional structures formed behind the cylinder significantly change the wake downstream and consequently modify the forces and pressure field on the cylinder. The paper by Sumner (2013) is a comprehensive review of the theme.

Downstream of the low aspect ratio cylinder, the wake is characterized by a pair of counter-rotating streamwise vortices originating from the free end and denominated tip-vortices, as first seen in Okamoto and Yagita (1973) and Kawamura et al. (1984). Additionally, Roh and Park (2003) showed that the tip vortices originate in the upstream region of the free end. On the other hand, the model presented by Lee (1997) for a very low aspect ratio cylinder showed "arch-type vortex" formation in the near-wake region. In this model, flow separating from the circumferential leading edge of the free-end surface does not reattach but becomes contiguous with the arch-type vortex forming behind the cylinder.

* Corresponding author.
E-mail address: rodolfo_tg@tpn.usp.br (R.T. Gonçalves).

http://dx.doi.org/10.1016/j.jfluidstructs.2014.11.003
0889-9746/

Nomenclature

ρ	water density
ω_y	mean transversal vorticity
ω_z	mean vertical vorticity
D	cylinder diameter
$C_x(t)$	non-dimensional streamwise force
$\overline{C_x}$	averaged mean non-dimensional streamwise force
$C_{x\,rms}$	non-dimensional streamwise force fluctuation
$C_y(t)$	non-dimensional transverse force
$C_{y\,rms}$	non-dimensional transverse force fluctuation
D	cylinder diameter
Fr_D	Froude number based on cylinder diameter
Fr_L	Froude number based on submersed cylinder length
f_s	vortex shedding frequency
$F_x(t)$	streamwise force
$F_y(t)$	transverse force
g	gravity acceleration
H	water level of the water channel
L	submersed cylinder length
L/D	aspect ratio
Re	Reynolds number
St	Strouhal number
U	incident flow velocity
U_x	mean streamwise velocity
U'_x	streamwise velocity fluctuation
U'_y	transverse velocity fluctuation
U'_z	vertical velocity fluctuation
W	water channel width
x	streamwise direction
y	transverse direction
z	vertical direction

Actually, another couple of counter-rotating streamwise vortices generated over the free end of a cylinder with $L/D=5$ were visualized by Park and Lee (2000) through a particle tracer technique and light sheet; these structures are detached from the separation region at the circumferential leading edge of the free end, one for each side of the wake, and they are counter-rotating with respect to the tip-vortices. These two couples of vortexes were visualized using the PIV – particle image velocimetry technique and can be found in Sumner et al. (2004), Adaramola et al. (2006) and Rostamy et al. (2012), for cylinders ranging from $3<L/D<9$; and Pattenden et al. (2005), for cylinder with $L/D=1$. More recently, Palau-Salvador et al. (2010) presented a comparison between experimental and numerical results (LES – large eddy simulations) for cylinders with $L/D=2.5$ and 5.

Some recent papers on the subject of the free-end flow by Roh and Park (2003), Pattenden et al. (2005) and Hain et al. (2008) showed a flow topology consisting of two pairs of counter-rotating streamwise vortices for cylinder with $1\leq L/D\leq 4.25$. The streamwise vorticity is thus important to low aspect ratio cylinders, and may be the source of the alternating forces since the low aspect ratio cylinders do not present von Kárman street, i.e., alternating vortex shedding. The numerical results by Rosetti et al. (2013), for a cylinder with $L/D=2$, showed the presence of two pair of vortices formed at the free end that fold around the trailing edge of the cylinder and are up-washed by the flow meeting the arch-type vortices. Those works emphasize the increasing importance of the free-end flow with reducing aspect ratio.

An interesting way to look at the flow around very low aspect ratio cylinders is looking at the flow around a hemispherical mounted-surface, e.g. in Taniguchi et al. (1982), Savory (1986) and Tamai et al. (1987). In this way, the recirculation region, or separation bubbles, behind the very low aspect ratio cylinder acts to alter the shape around it to become similar to a hemispheric. This favors the formation of the arch-type vortex (see Lee, 1997). In the hemispheric case, arched tubes formed behind the hemisphere, several of the tubes coalesced and shedding; this behavior is responsible for an alternating force in the transverse direction. Analogous behavior can be attributed to very low aspect ratio cylinders if the same model proposed by Lee (1997) is used. The works on VIV of spheres can also help to understand the VIV of low aspect ratio cylinders (see Govardhan and Williamson, 1997, 2005; Jauvtis et al., 2001; Schouveiler and Provansal, 2002), since the main source of the forces in the transverse direction is due to the interaction of the trailing vortices with streamwise vorticity.

In the offshore scenario, the low aspect ratio cylinders have attracted attention due to the increasing size of the circular platforms, such as spar and monocolumn. The current incidence around these types of platforms promotes the phenomenon of VIM – vortex-induced motion. VIM causes vortex-shedding around the platforms and, consequently, motion amplitudes of the order of the characteristic length of the body subject to VIM in the horizontal plane. Another important VIM characteristic is the low aspect ratio of these systems, i.e. $L/D<6$. Spar platforms ranging from $1.5<L/D<6$ (see examples in van Dijk et al., 2003; Roddier et al., 2009); monocolumn platforms ranging from $0.2<L/D<0.5$ (see examples in Cueva et al., 2006; Gonçalves et al., 2010); and aspect ratio of semi-submersible columns ranging from $0.4<L/D<3$ (see examples in Waals et al., 2007; Gonçalves et al., 2012a). The aspect ratio of these systems confirms the importance of better understanding the flow around finite height cylinders. More details about the VIM in offshore platforms can be found in detail in Fujarra et al. (2012). On the other hand, fundamental works about VIV of low aspect ratio cylinders are few in the literature, among which Someya et al. (2010), Gonçalves et al. (2012b, 2013), Rahman and Thiagarajan (2013) and Zhao and Cheng (2014) can be highlighted.

In the offshore scenario described previously, the cylindrical structures pierce the free surface. The flow around surface-mounted cylinders and cylinders piercing free surface are different due to the boundary conditions. In the first one, the cylinder can be immersed in the boundary layer formed at the surface bottom, and also the bottom can be considered a

stationary boundary condition; in the latter, the boundary condition is moving due to the free surface and it can change at high velocities due to wave formation.

There are few works about flow around stationary cylinders considering the free-surface effects in the wake. Hay (1947) studied low aspect ratio cylinders piercing the free surface and also studied the influence of the free surface on the forces acting in the cylinder and the water elevation, behind and in front of the cylinder. But the author did not study the vortex shedding effects. The work by Hay showed the effect of the aspect ratio in the water elevation around the cylinder and the importance of considering a Froude number based on the submersed length of the cylinder $\mathrm{Fr}_L = U/\sqrt{gL}$. They reported a superior limit of $\mathrm{Fr}_L = 0.5$ in which the free-surface effects can be neglected. More recently, Chaplin and Teigen (2003) showed that the total force coefficient reaches a maximum at a $\mathrm{Fr}_D = U/\sqrt{gD}$ of about 1 when the free-surface effects are considered for a large draught cylinder in a steady current.

In this work, stationary low aspect ratio cylinders piercing the free surface were investigated using PIV measurements. Special focus was placed on the flow around the free end and immediately behind the cylinder where the flow recirculates. Another approach was taken to understand the aspect ratio influence on the forces around the cylinder (streamwise, x, and transverse, y, directions) and vortex-shedding frequency. The last study was carried out using force measurements. The greatest difference between the present work and the ones presented in the literature is the extremely low aspect ratio tested, ranging from $0.1 \leq L/D \leq 2.0$, and the pierced free-surface characteristic of the cylinder.

2. Experimental setup

All the experiments were carried out in a recirculating water channel at the NDF – Fluid & Dynamics Research Group Laboratory facility of USP – University of São Paulo, Brazil. The dimension of the test section is $7500 \times 700 \times 700$ mm^3 and the flow has low levels of turbulence (less than 2%) with free-stream velocities up to 0.40 m/s. Further details concerning the water channel can be found in Assi et al. (2005).

The model was made of PVC – polyvinyl chloride with external diameter $D = 125$ mm and was placed at the centerline of the channel. A 6dof – degree-of-freedom – load cell ATI, Mini40 model, was used to acquire the hydrodynamic forces. The uncertainty of the measured forces was 1/200 N, with absolute forces ranging from 1/125 N up to 2.5 N. The data was acquired along 180 s with sample frequency of 100 Hz. Fig. 1 presents a scheme of the experimental arrangement.

Two-dimensional PIV was used aiming at quantifying the flow around the cylinder. 345 snapshots were acquired at a 14.8 Hz sample frequency. The optical system was composed of a Nikon lens, model AF Nikkor $f/1.4D$ with focal length 50 mm, an Imager Pro X2 Megapixel camera and a Quantel (Brilliant Twins) double-cavity pulsed Nd:YAG laser system (532 nm wavelength). The water was seeded with polyamide particles about 11 μm in diameter and density close to 1030 kg/m^3. The vector fields were calculated using the DaVis 7.2 software, employing a two-pass windowing process with decreasing size. The first step employed a 64×64 pixel interrogation window and the second step concerned a correlation

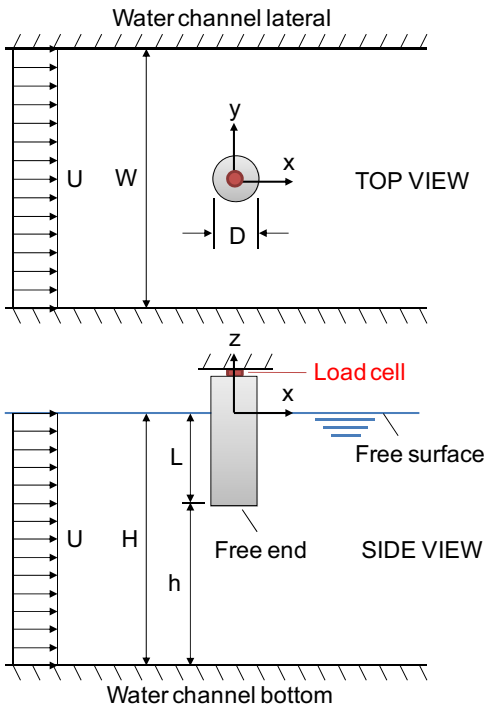

Fig. 1. Experimental setup and dimensional parameters for force measurement tests.

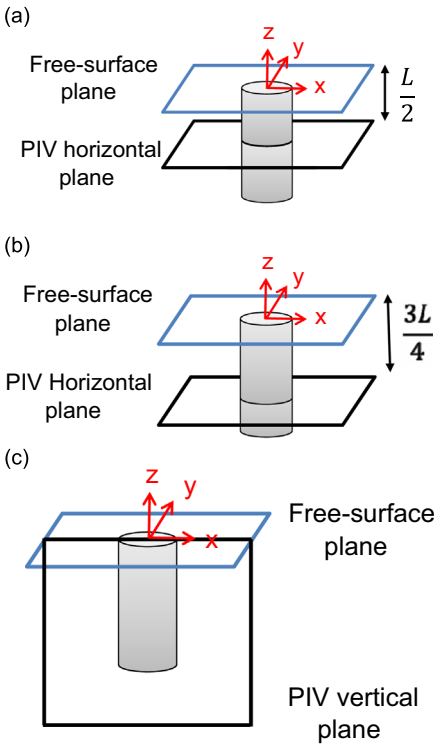

Fig. 2. PIV measured plane positions: (a) horizontal mid-span plane at $z/L=-0.5$, (b) horizontal plane near the cylinder free end at $z/L=-0.75$ and (c) vertical center plane at $y/D=0$.

with a 32×32 pixel window. Further details regarding the PIV facility can be found in Korkischko and Meneghini (2011).

Three different planes were chosen to be measured: two horizontal planes, namely one mid-span plane at $z/L=-0.5$ and one near the free end at $z/L=-0.75$, and one vertical plane, namely one center plane at $y/D=0$ (see details in Fig. 2).

The free-end cylinder was kept constant above the water channel bottom, the distance between the cylinder free end and the channel bottom was around $h=460$ mm, i.e. larger than $3.5D$ sufficient for there being no boundary layer effect due to the bottom. The changes in the aspect ratio were made by changing the water level, H. The blockage of the experiments was $D/W=0.18$, where W is the water channel width, value below the critical blockage value of 0.2, as presented in Griffith et al. (2011).

3. Experimental results

In this section, the experimental results from load cell measurements and PIV are presented.

3.1. Force measurements

The streamwise, $C_x(t)$, and transverse, $C_y(t)$, non-dimensional forces are defined as

$$C_x(t)=\frac{2F_x(t)}{\rho LDU^2}, \tag{1}$$

$$C_y(t)=\frac{2F_y(t)}{\rho LDU^2}, \tag{2}$$

where $F_x(t)$ and $F_y(t)$ are the streamwise and transverse forces, respectively

The vortex-shedding frequency, f_s, was inferred from the frequency related to the largest peak energy in the PSD – power spectrum density of the $C_y(t)$; thus, the Strouhal number can be calculated as

$$\mathrm{St}=\frac{f_sD}{U}. \tag{3}$$

The original signal from the load cell was filtered using a windowing process to avoid very high and very low frequencies, which are not physically meaningful. The interest frequencies range from 0.05 Hz up to 1 Hz.

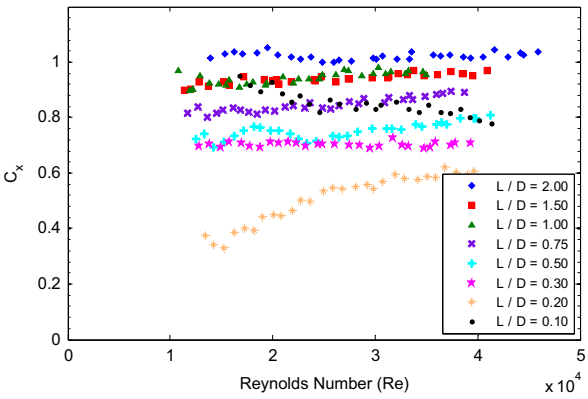

Fig. 3. C_x values in function of Reynolds number for each cylinder aspect ratio.

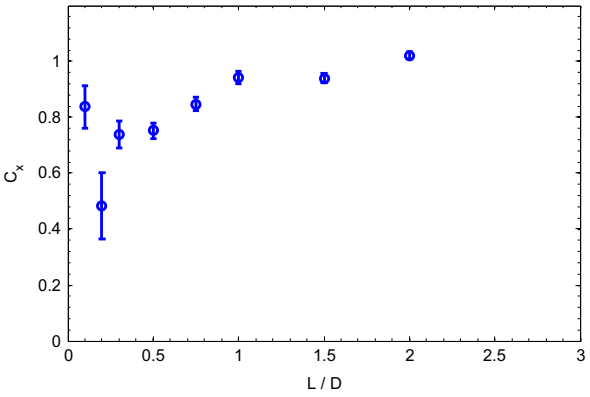

Fig. 4. Averaged $\overline{C_x}$ values and respective standard deviation for a range of $10\,000 < \mathrm{Re} < 50\,000$ in function of cylinder aspect ratio.

Forty different velocities of the incoming flow were carried out for each aspect ratio of the cylinder. The velocities corresponded to a range of $10\,000 < \mathrm{Re} < 50\,000$. The mean streamwise force coefficient, as well as the root-mean-square of force coefficients (streamwise and transverse directions) and Strouhal number were evaluated for each Re condition. The mean streamwise force coefficient in function of the Reynolds number for each cylinder aspect ratio is presented in Fig. 3. The averaged mean streamwise force coefficient and its respective error bars that represent the standard deviation or the spread of the data, over the range of the Reynolds number, are presented in Fig. 4 with respect to aspect ratio. The same procedure was applied to other coefficients.

The values of $\overline{C_x}$ decrease with decreasing aspect ratio, except for $L/D = 0.1$, as presented in Fig. 4. The standard deviations are larger for the lowest aspect ratios, $L/D = 0.2$ and 0.1. This can be explained due to the high value of Fr_L in those aspect ratio conditions, $\mathrm{Fr}_L > 0.5$. As discussed in Hay (1947), the free-surface resistance force increase from $\mathrm{Fr}_L = 0.5$. The $\overline{C_x}$ is approximately $\overline{C_x} \sim 1$ and $\overline{C_x} \sim 0.7$ for $L/D = 2$ and 0.3, respectively. The typical value for infinite cylinder is $\overline{C_x} \sim 1$, as presented in Khalak and Williamson (1996), for $4000 < \mathrm{Re} < 12\,000$; on the other hand, in Iungo et al. (2012), a value of $\overline{C_x} \sim 0.8$ was obtained for a surface-mounted cylinder, $L/D = 3$ and $50\,000 < \mathrm{Re} < 113\,000$.

The values of non-dimensional streamwise force fluctuation $\overline{C_{x\,rms}}$ are practically constant, $\overline{C_{x\,rms}} \sim 0.1$ for cylinders with $0.75 \leq L/D \leq 2$, but with a decrease for $L/D < 0.5$, as presented in Fig. 5. This behavior can be explained by the changes in the wake characteristics for $L/D < 0.5$. This fact can be better discussed together with PIV and PSD results.

The values of non-dimensional transverse force fluctuation $\overline{C_{y\,rms}}$ are practically constant, $\overline{C_{y\,rms}} \sim 0.06 \pm 0.01$ for cylinders with $0.75 \leq L/D \leq 2$, but with a decrease for $L/D < 0.5$, as presented in Fig. 6. The typical value for infinite cylinder is $\overline{C_{y\,rms}} \sim 0.05$ for $6000 < \mathrm{Re} < 13\,000$, as presented in Khalak and Williamson (1996).

The values of averaged St showed a marked decrease with decreasing aspect ratio, as presented in Fig. 7. This behavior was observed by other authors; e.g. Sakamoto and Arie (1983) reported a decrease in St when the free end approached. The works by Fox and West (1993) and Park and Lee (2000) also reported this behavior. Sumner et al. (2004) found a value of $\mathrm{St} \approx 0.16$ for cylinders with $3 < L/D < 9$, and Iungo et al., (2012) of $\mathrm{St} \approx 0.15$ for $L/D = 3$. Moreover, the value $\mathrm{St} \approx 0.07$ was reported by Iungo et al. (2012) for measurements carried out near the cylinder free end.

The results of PSD help to better understand the free-end effects. The PSD of the non-dimensional forces for $L/D = 2.0$ is presented in Fig. 8(a). It is possible to identify a dominant frequency, $\mathrm{St} \sim 0.15$, for the transverse force in the PSD of C_y. This frequency is due to an alternated vortex shedding and this is not Re dependent. On the other hand, for the streamwise force,

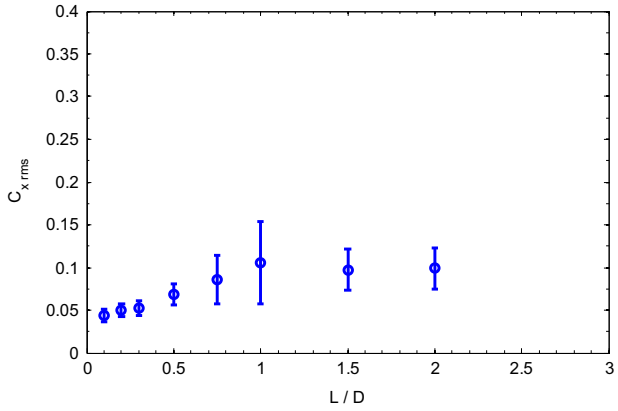

Fig. 5. Averaged $C_{x\,rms}$ values and respective standard deviation for a range of $10\,000 < \mathrm{Re} < 50\,000$ in function of cylinder aspect ratio.

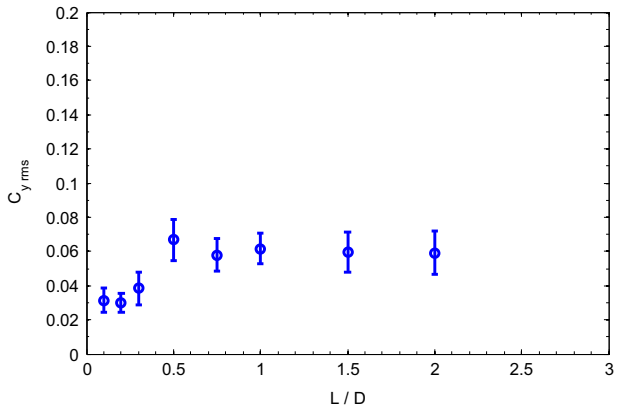

Fig. 6. Averaged $C_{y\,rms}$ values and respective standard deviation for a range of $10\,000 < \mathrm{Re} < 50\,000$ in function of cylinder aspect ratio.

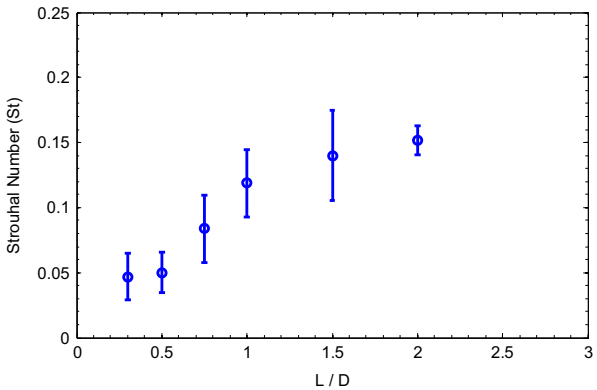

Fig. 7. Averaged St values and respective standard deviation for a range of $10\,000 < \mathrm{Re} < 50\,000$ in function of cylinder aspect ratio.

the PSD energy is concentrated in a low frequency range, $\mathrm{St} < 0.1$, as compared with the results for the transverse force. This frequency is also due to an alternated vortex shedding and is Re dependent.

The behavior of the PSD of the non-dimensional transverse force for $0.75 \leq L/D \leq 1.5$, presented in Fig. 8(b)–(d), is disperse, yet it can identify a dominant frequency for each case. The dominant frequency is lowered by decreasing the aspect ratio. In the same PSD, the presence of lower frequencies can be observed in the same range of the streamwise force. In these cases, the streamwise dominant frequency has the same behavior presented for $L/D = 2.0$.

The dominant frequencies in the PSD for $L/D = 0.5$ (see Fig. 9(a)), are in the same frequency range and occur simultaneously in the transverse and streamwise directions. For $L/D = 0.3$, presented in Fig. 9(b), it still is possible to

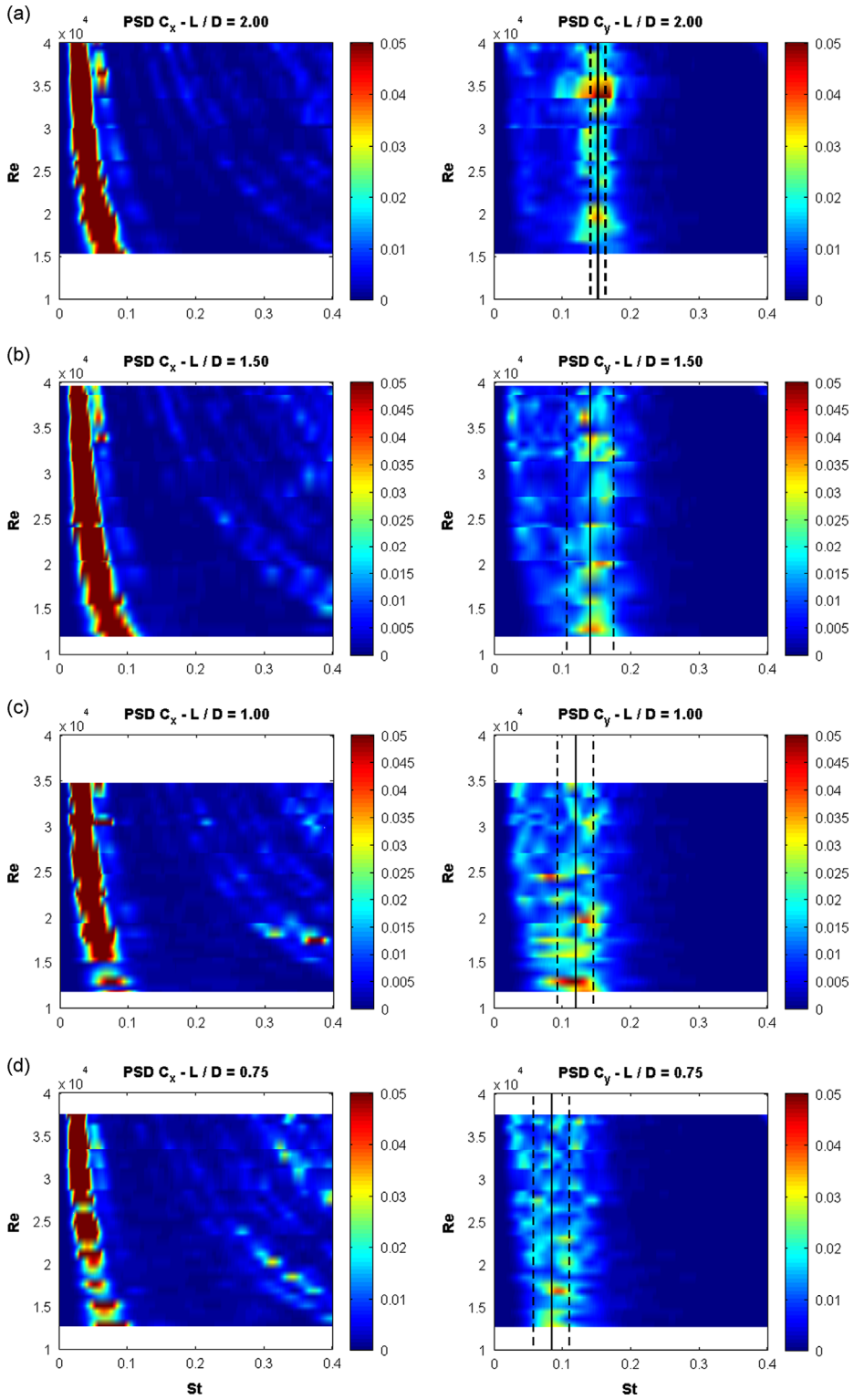

Fig. 8. PSD distribution for force in the streamwise direction (on the left) and in the transverse direction (on the right) in function of Re and St for cylinder with different aspect ratios: (a) $L/D = 2.0$, (b) $L/D = 1.5$, (c) $L/D = 1.0$ and (d) $L/D = 0.75$.

identity a dominant transverse frequency, but lower than for higher aspect ratio cylinders. Finally, for $0.1 \leq L/D \leq 0.2$ (see Fig. 9(c)–(d)), there is no significant energy in the PSD of the transverse force and there is only some energy in the streamwise direction.

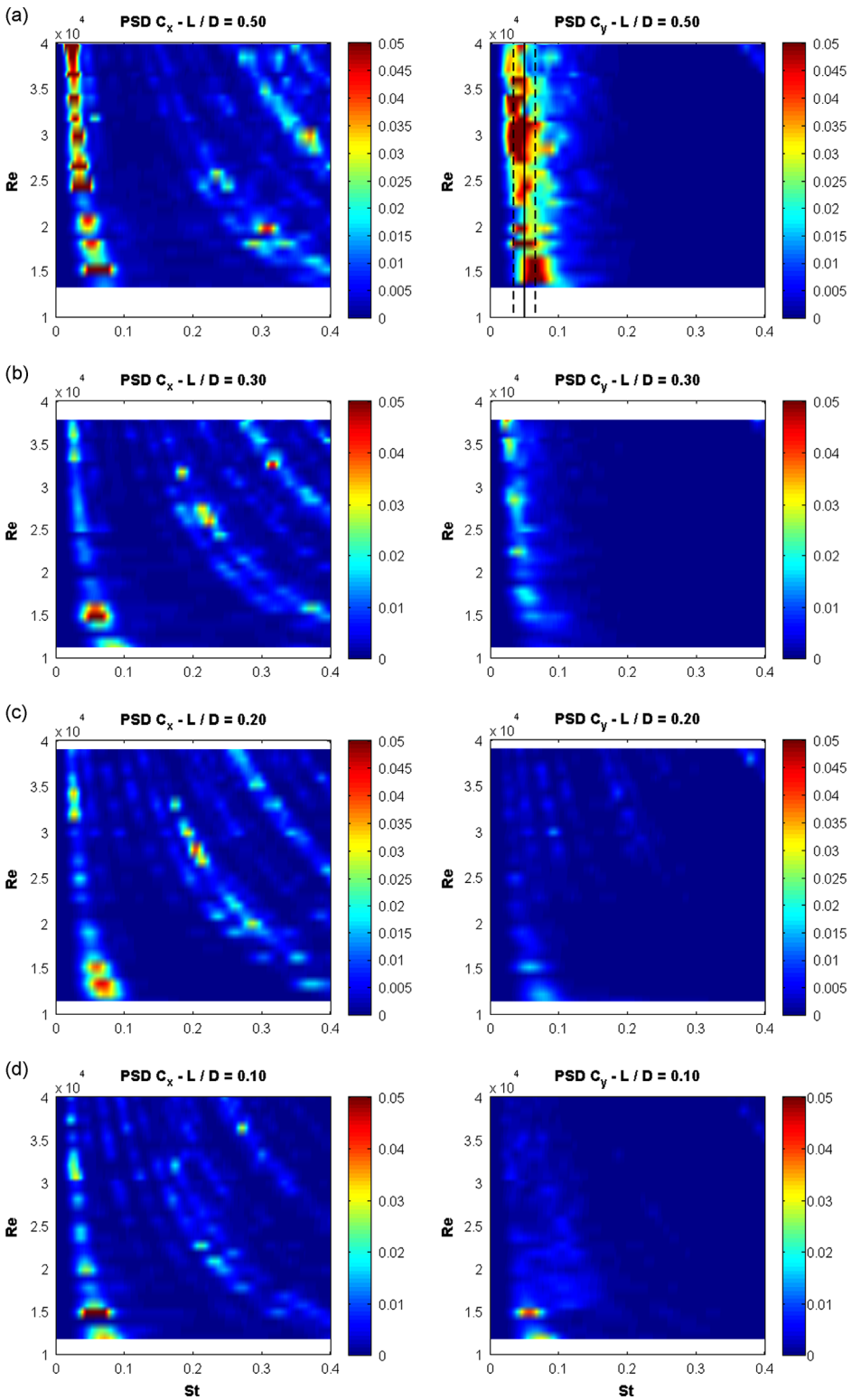

Fig. 9. PSD distribution for force in the streamwise direction (on the left) and in the transverse direction (on the right) in function of Re and St for cylinder with different aspect ratios: (a) $L/D = 0.5$, (b) $L/D = 0.3$, (c) $L/D = 0.2$ and (d) $L/D = 0.1$.

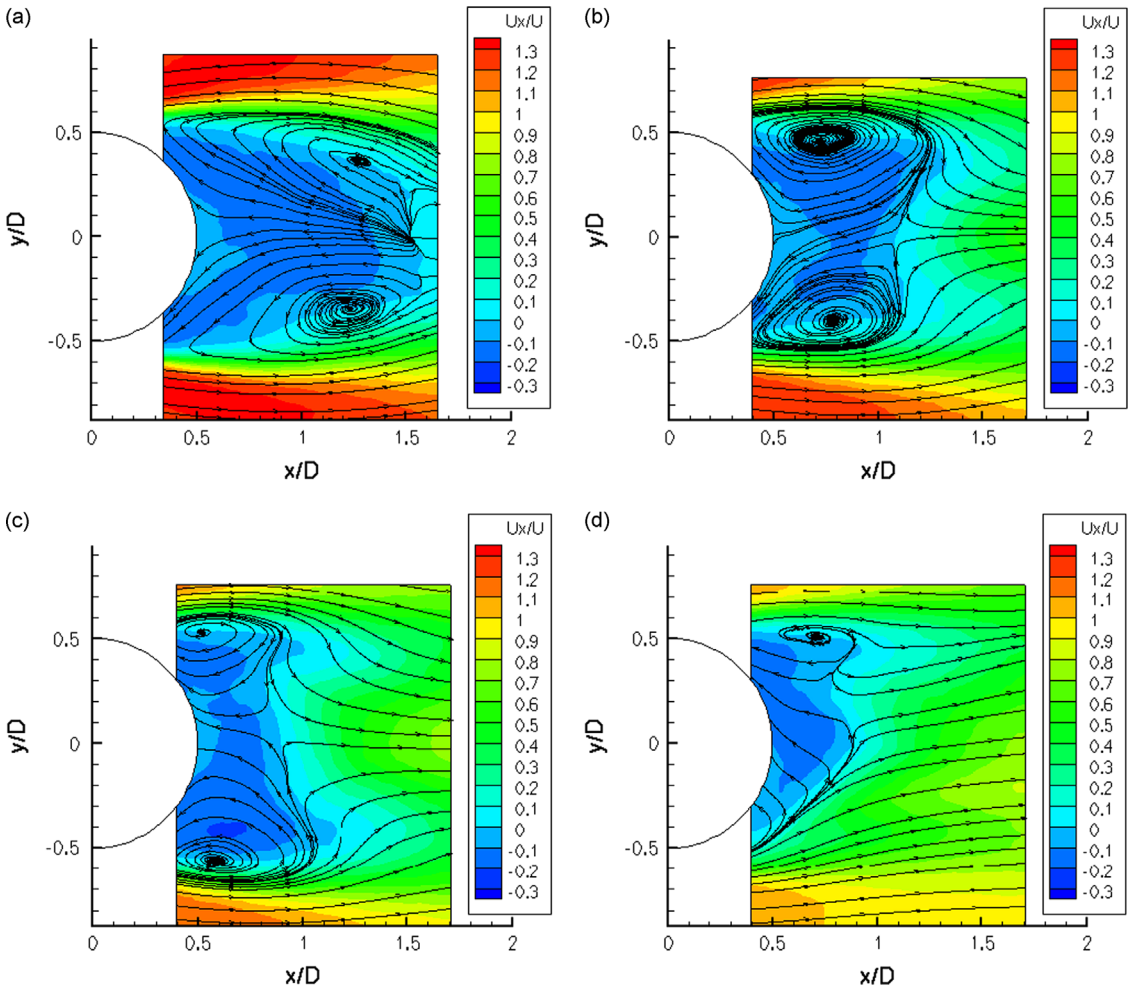

Fig. 10. Time-average streamlines and contours of mean velocity component U_x/U in the horizontal plane at $z/L=-0.5$ for Re=43 000: (a) $L/D=2.0$, (b) $L/D=1.0$, (c) $L/D=0.5$ and (d) $L/D=0.3$.

Table 1
Position of the core of the horizontal recirculation region (bubbles) behind the cylinder in function of aspect ratio.

Work	L/D	x/D	y/D
Present work	0.3	–	–
	0.5	0.5–0.6	0.5–0.6
	1.0	0.7–0.8	0.4
	2.0	1.2–1.3	0.35
Palau-Salvador et al. (2010)	2.5	1.4	0.35–0.4
	5.0	1.6	0.3–0.35

These results showed that the dominant frequency in the streamwise direction is Reynolds dependent, i.e. the dominant frequency decreases with increasing Re and occurs in a specific range of $St<0.1$. However, this frequency does not change with the aspect ratio, which permits to conclude that the behavior is due to the presence of the cylinder free end.

The vortex shedding structures can be dominated by a von Kármán street characteristics (repeating pattern of swirling vortices caused by the unsteady separation of the flow around the cylinder in the horizontal plane) for $L/D=2.0$, in which $St\sim0.15$ can be well defined. This value is similar to that obtained by Iungo et al. (2012) for $L/D=3.0$.

In the range of $0.75\leq L/D\leq1.5$, we can conjecture that the influence of the structures formed due to the presence of the cylinder free end grows. This behavior affects the PSD of the transverse force, including energy in the same low frequencies

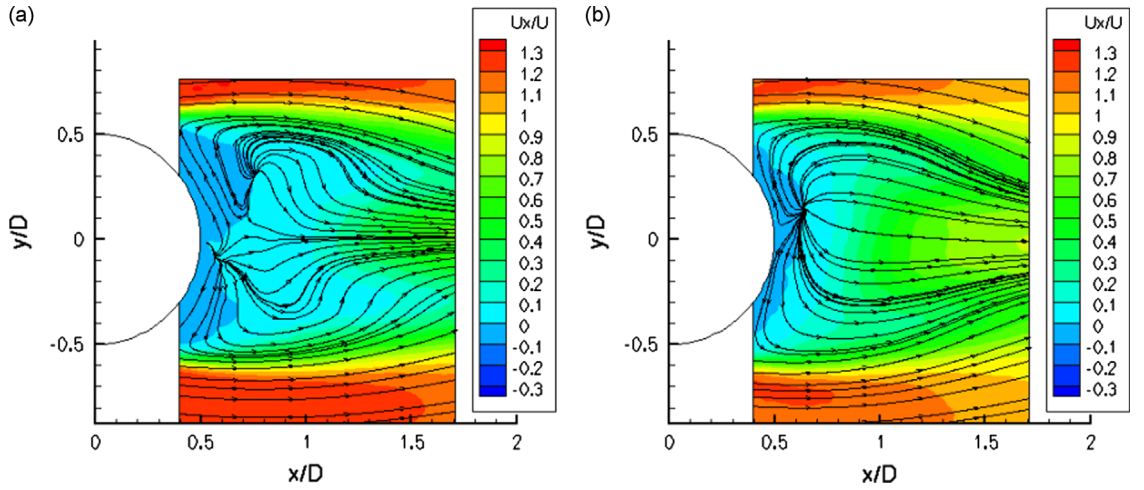

Fig. 11. Time-average streamlines and contours of mean velocity component U_x/U in the horizontal plane at $z/L=-0.75$ for Re=43 000: (a) $L/D=2.0$ and (b) $L/D=1.0$.

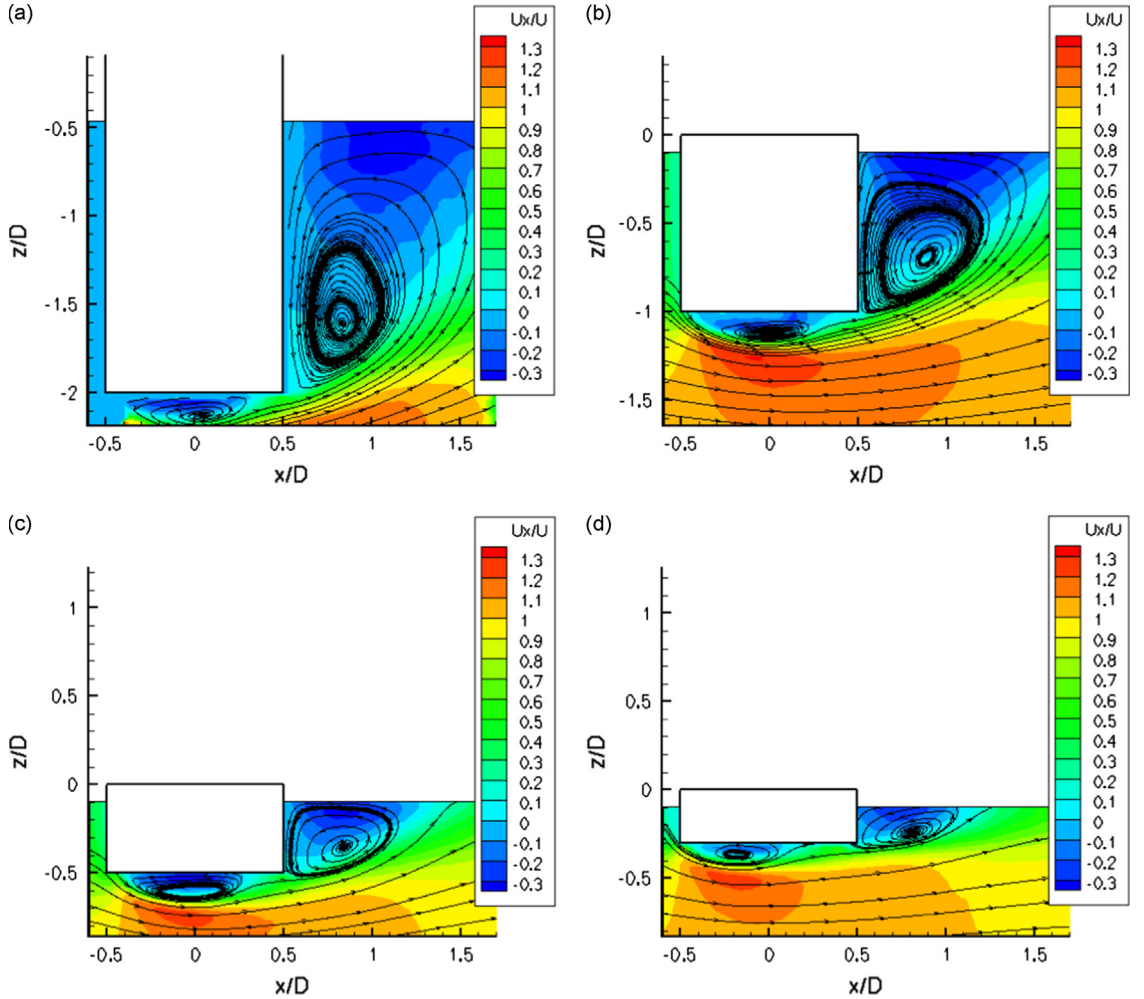

Fig. 12. Time-average streamlines and contours of mean velocity component U_x/U in the vertical center plane at $y/D=0$ for Re=43 000: (a) $L/D=2.0$, (b) $L/D=1.0$, (c) $L/D=0.5$ and (d) $L/D=0.3$.

Table 2
Reattachment positions in the vertical plane in function of aspect ratio.

Work	L/D	x/D
Present work	0.3	1.1
	0.5	1.2
	1.0	1.8
	2.0	>1.8
Palau-Salvador et al. (2010)	2.5	3.0
	5.0	3.6

Table 3
Position of the core of the longitudinal recirculation region behind the cylinder in function of aspect ratio.

Work	L/D	x/D	$\lvert z/D\rvert$	$\lvert z/L\rvert$
Present work	0.3	0.8	0.2	0.7
	0.5	0.8–0.9	0.3	0.6
	1.0	0.9	0.6–0.7	0.6–0.7
	2.0	0.8–0.9	1.6	0.8
Palau-Salvador et al. (2010)	2.5	0.8	2.0	0.8
	5.0	0.9	4.0	0.8

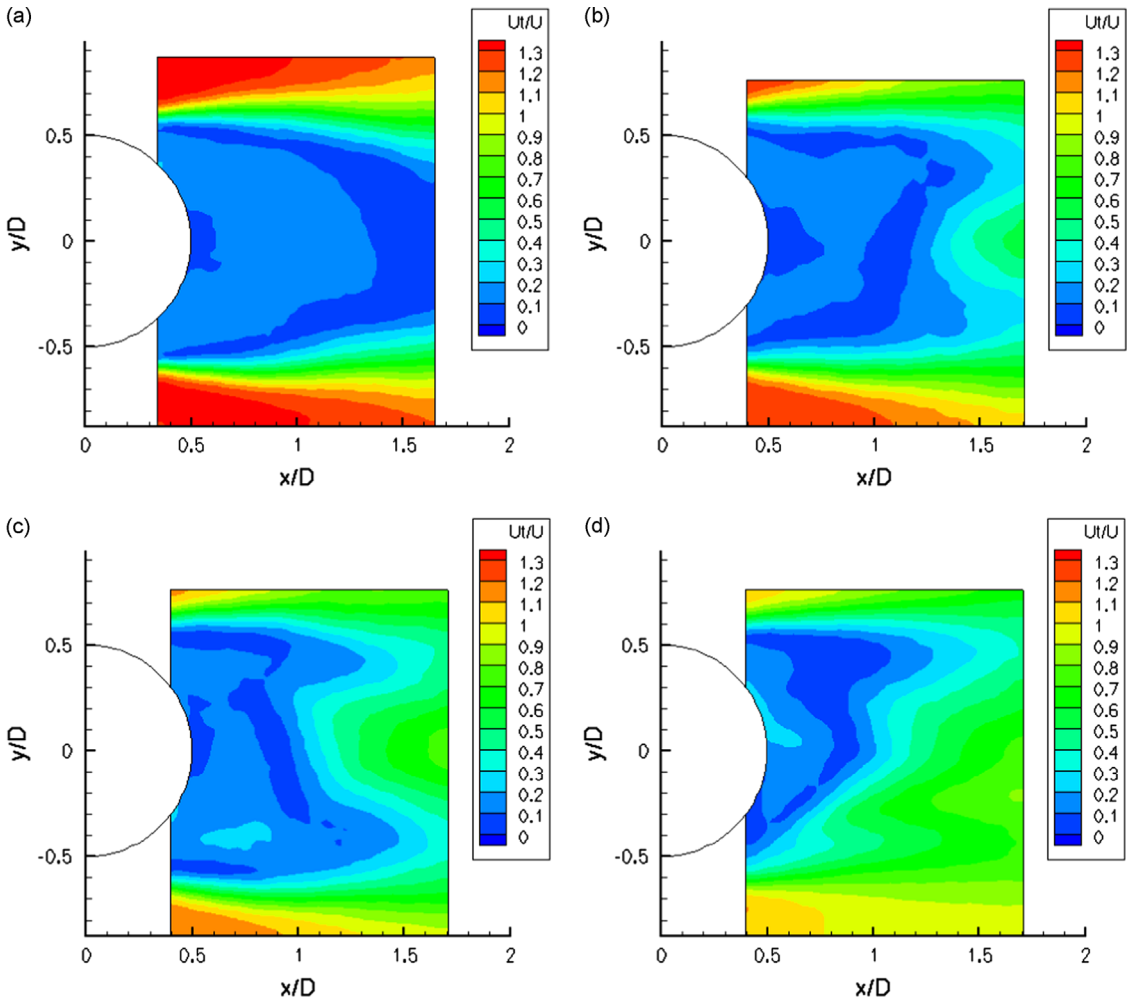

Fig. 13. Contours of mean total velocity $\boldsymbol{U_t}/\boldsymbol{U}$ in the horizontal plane at $z/L=-0.5$ for Re=43 000: (a) $L/D=2.0$, (b) $L/D=1.0$, (c) $L/D=0.5$ and (d) $L/D=0.3$.

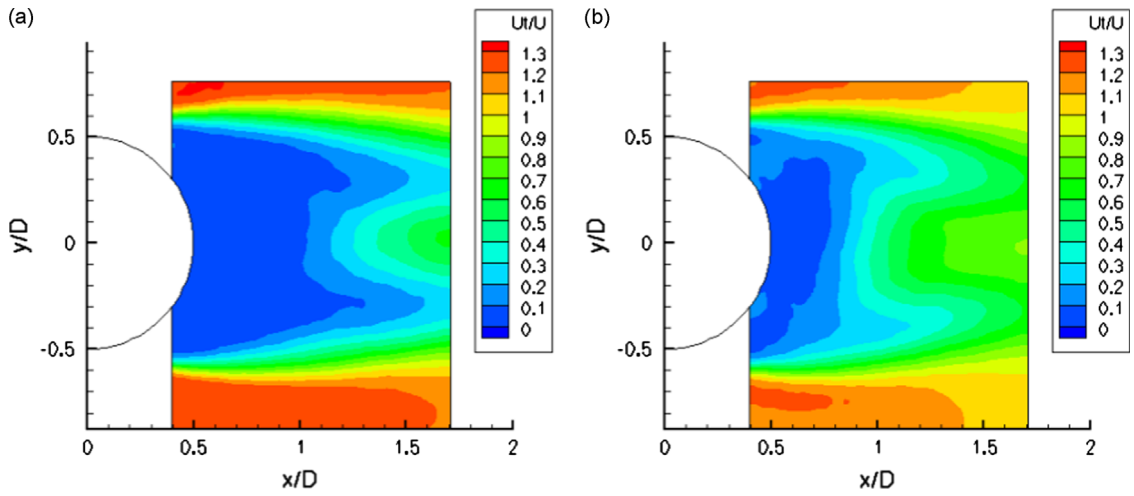

Fig. 14. Contours of mean total velocity U_t/U in the horizontal plane at $z/L=-0.75$ for Re=43 000: (a) $L/D=2.0$ and (b) $L/D=1.0$.

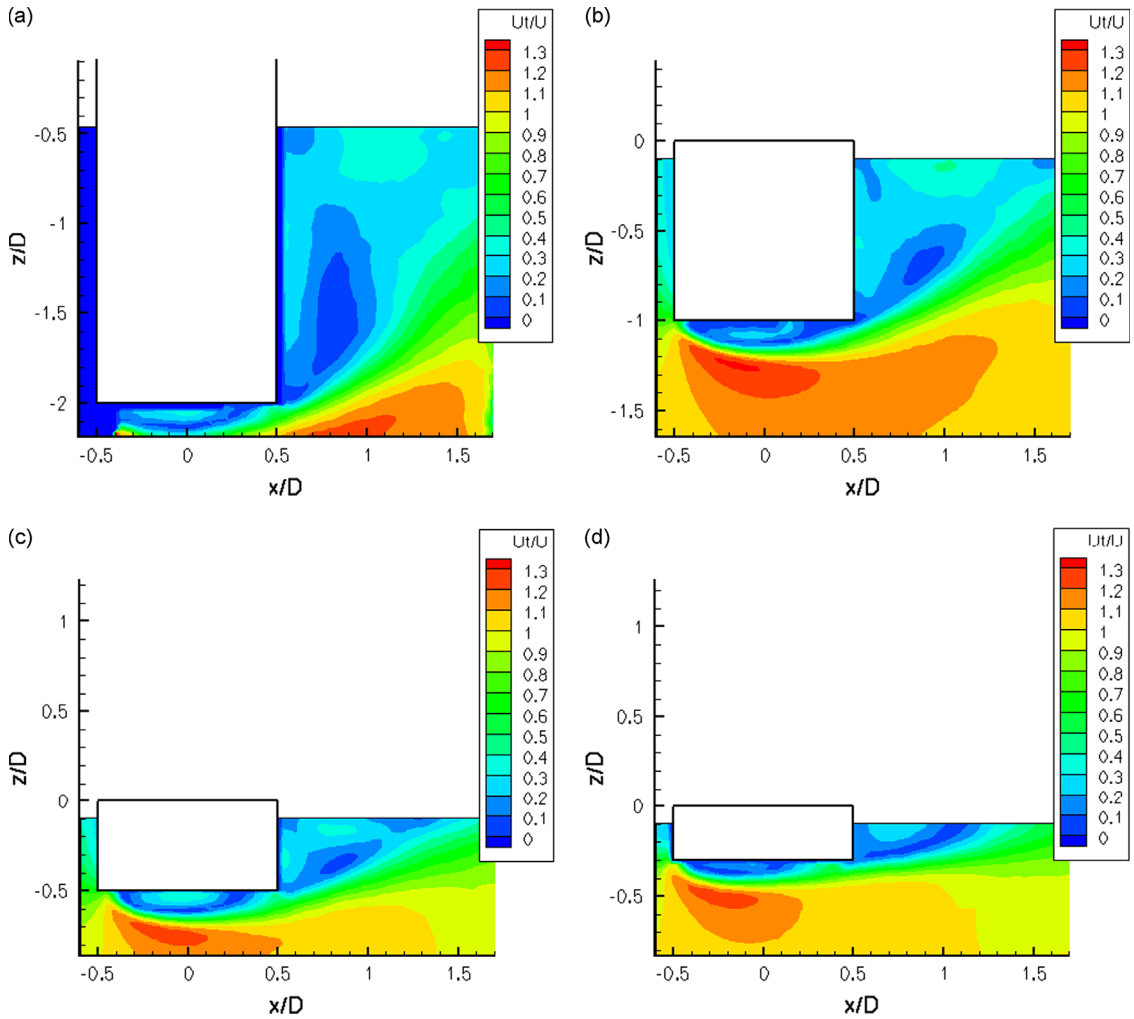

Fig. 15. Contours of mean total velocity U_t/U in the vertical center plane at $y/D=0$ for Re=43 000: (a) $L/D=2.0$ and (b) $L/D=1.0$.

as those in the streamwise direction. Therefore, less regularity of the vortex shedding was observed by decreasing the aspect ratio and the structures due to the cylinder free end beginning to contaminate the wake.

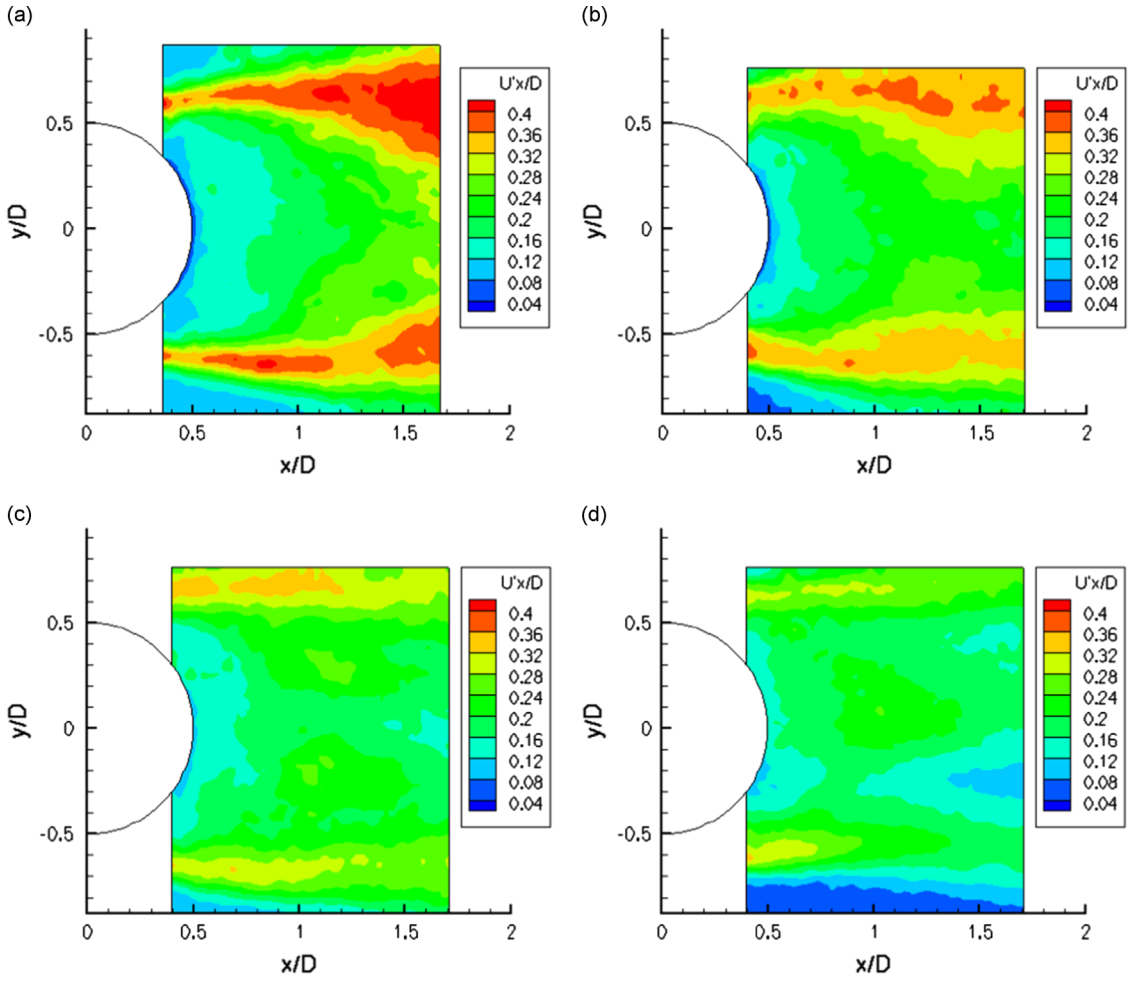

Fig. 16. Contours of root mean square of streamwise fluctuations U'_x/U in the horizontal plane at $z/L=-0.5$ for Re=43 000: (a) $L/D=2.0$, (b) $L/D=1.0$, (c) $L/D=0.5$ and (d) $L/D=0.3$.

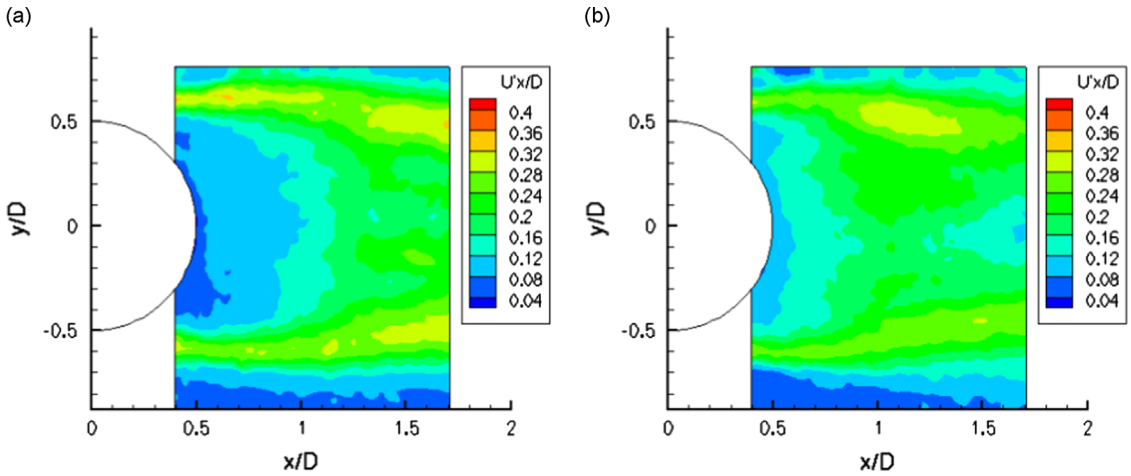

Fig. 17. Contours of root mean square of streamwise fluctuations U'_x/U in the horizontal plane at $z/L=-0.75$ for Re=43 000: (a) $L/D=2.0$ and (b) $L/D=1.0$.

For $L/D=0.5$, there are not two frequencies in the transverse direction, but only one that is the same as that in the streamwise direction. This frequency is due to the vortex shedding around the cylinder free end. The wake characteristics in these range of aspect ratio are only due to the cylinder free end and can be comparable to the arch-typed vortex, i.e. arched tubes were formed in behind the low aspect ratio cylinder, see similar model proposed by Lee (1997). These structures can be responsible for the alternated forces even for low aspect ratio cylinders. The PIV results presented further on here can complement this conjecture.

For $L/D=0.2$, there is no significant energy force in the transverse direction; in this aspect ratio, the structures formed around the cylinder free end are not able to produce alternating forces. This fact shows $L/D=0.2$ is a critical value in terms of transverse forces. Therefore, the behavior for $L/D<0.5$ (see Figs. 4, 5, 7 and 9) can confirm characteristic changes due to dominant three-dimensional effects in the presence of the cylinder free end.

3.2. PIV measurements

In this section, the results from the PIV measurements are presented for Re=43 000. Three different planes were visualized for cylinders with $L/D=2.0$, 1.0, 0.5 and 0.3. Two horizontal planes, namely one mid-span plane at $z/L=-0.5$ and one near the free end at $z/L=-0.75$, and one vertical center plane at $y/D=0$. Time-averaged mean velocities and turbulence quantities from the PIV measurements are presented and compared for all aspect ratio cylinders. All mean and fluctuating velocities were made non-dimensional with the incident flow velocity U. The turbulence or fluctuating velocities are calculated as the root-mean-square of the time histories of velocity.

Fig. 10 shows contours of the mean streamwise velocity U_x/U together with streamlines in the horizontal plane at mid-span length of the cylinder at $z/L=-0.5$. The streamlines for $L/D=2.0$ show the typical picture of the flow around a circular cylinder, i.e. separation from the stagnation point and the formation of a recirculation region on either side of the

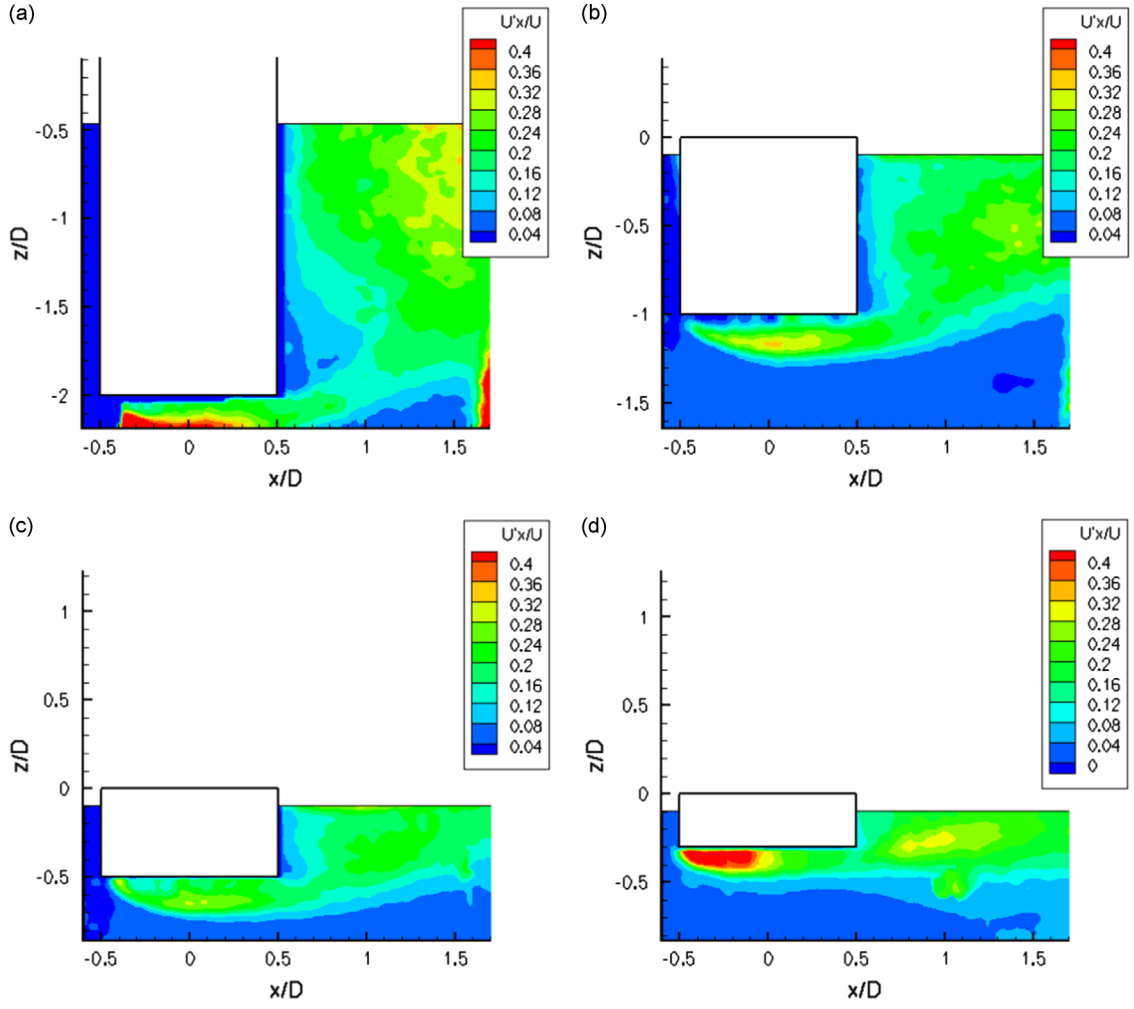

Fig. 18. Contours of root mean square of streamwise fluctuations U'_x/U in the vertical center plane at $y/D=0$ for Re=43 000: (a) $L/D=2.0$, (b) $L/D=1.0$, (c) $L/D=0.5$ and (d) $L/D=0.3$.

symmetry plane. The recirculation region length at mid-span length reduces significantly with the decreasing aspect ratio, as can be seen in Table 1, including the results for the mounted-surface cylinders by Palau-Salvador et al. (2010). For $L/D=0.5$, a fairly clear recirculation region still exists, but the recirculation region length is reduced. The effects of the free end are clearly present already and they are much stronger for the lowest aspect ratio cylinder, in which the free-end effects on the longitudinal recirculation region distort the recirculation region in the horizontal plane. For $L/D=0.3$, it is difficult to find recirculation regions in the horizontal plane.

Fig. 11 shows contours of the mean streamwise velocity U_x/U in the horizontal plane near the free end at $z/L=-0.75$ for $L/D=2.0$ and 1.0. This plane is near the position of the longitudinal recirculation region at $z/L\sim-0.8$. In this region, the free-end effects disturb the horizontal recirculation region; due to this, the recirculation regions are smaller. The same effect was presented by Palau-Salvador et al. (2010) for $L/D=50.0$ and 2.5.

Fig. 12 shows contours of the mean streamwise velocity U_x/U together with streamlines in the vertical center plane at $y/D=0$. The incident flow moves below the free-end cylinder, separating at the leading edge. Behind the cylinder, a large longitudinal recirculation region is observed for both cases, but the reattachment of the separated flow on the free surface varies with L/D. The reattachment positions for each L/D can be seen in Table 2, including the results for the mounted-surface cylinders by Palau-Salvador et al. (2010).

The core of the longitudinal recirculation region also varies with L/D, but it is positioned closer to the free end at $x/D\sim0.85$ and $|z/L|\sim0.7$, as can be seen in Table 3.

Figs. 13–15 show contours of mean total velocity U_t/U in the horizontal plane at $z/L=-0.50$, in the horizontal plane at $z/L=-0.75$ and in the vertical plane at $y/D=0$. These figures confirm the large recirculation region behind the cylinder in both planes.

Figs. 16 and 19 show contours of streamwise, U'_x/U, and transversal, U'_y/U, fluctuations in the horizontal mid-span length plane, respectively. For $L/D=2.0$, starting from the point of the flow detachment from the cylinder wall, a separated shear layer develops bordering the separation bubble; and in this shear layer, streamwise fluctuations are generated by

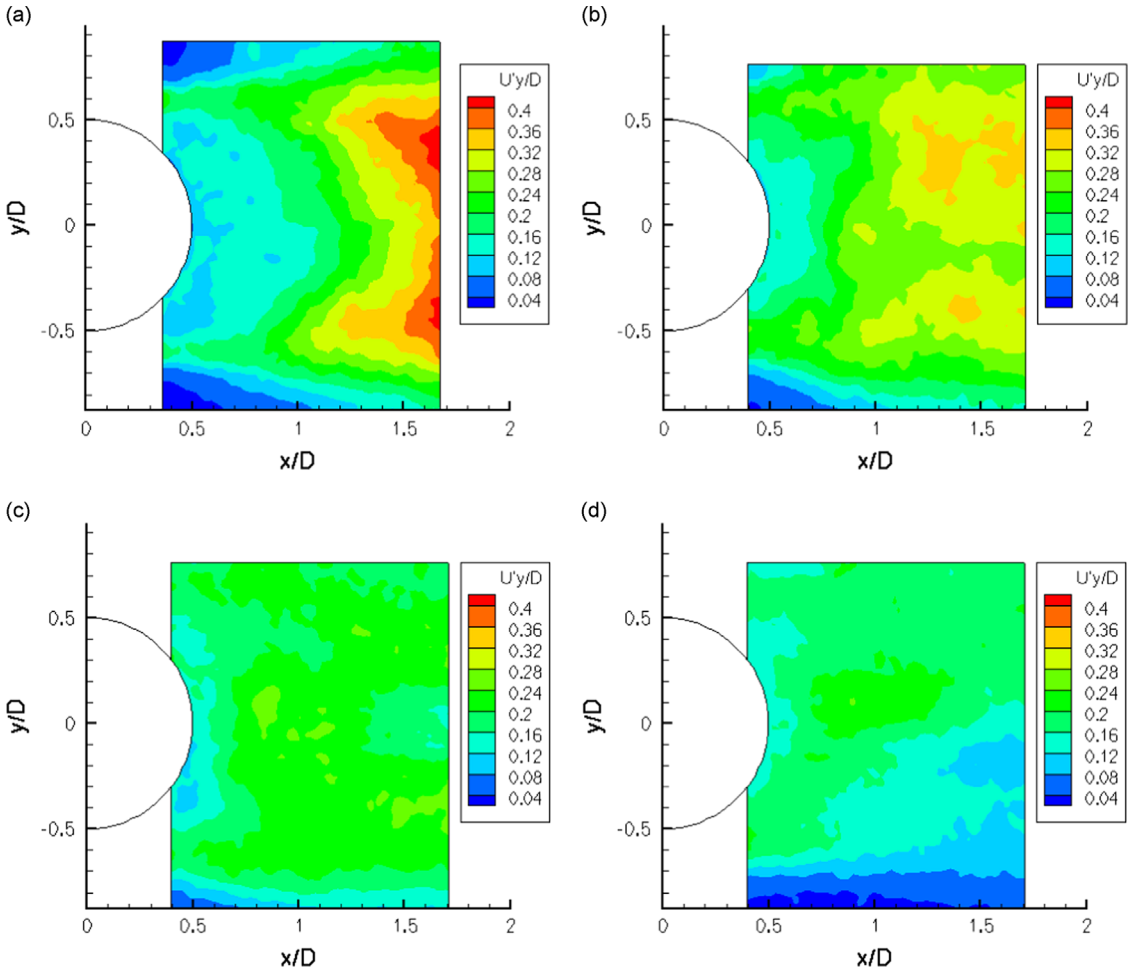

Fig. 19. Contours of root mean square of transverse fluctuations U'_y/U in the horizontal plane at $z/L=-0.5$ for Re=43 000: (a) $L/D=2.0$, (b) $L/D=1.0$, (c) $L/D=0.5$ and (d) $L/D=0.3$.

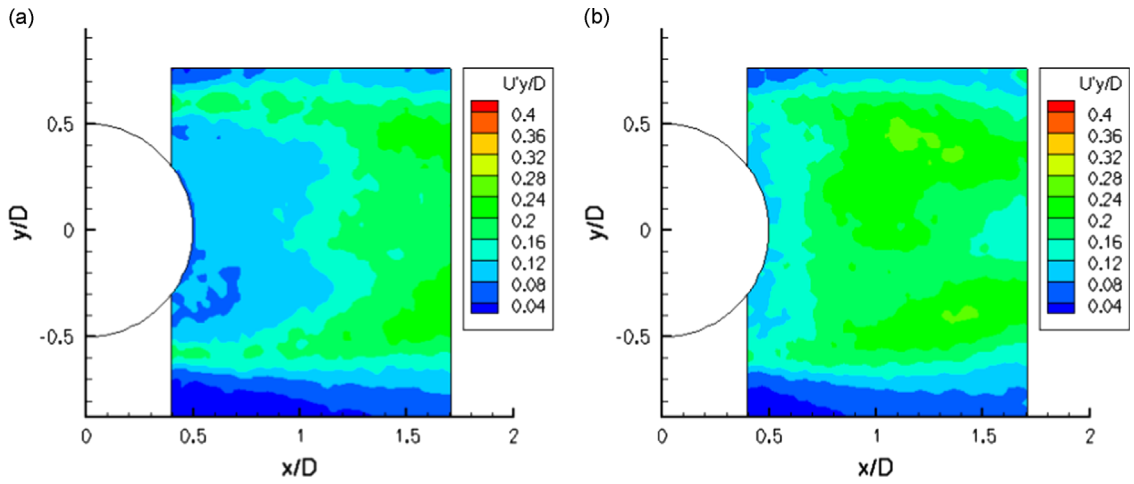

Fig. 20. Contours of root mean square of transverse fluctuations U'_y/U in the horizontal plane at $z/L=-0.75$ for Re=43 000: (a) $L/D=2.0$ and (b) $L/D=1.0$.

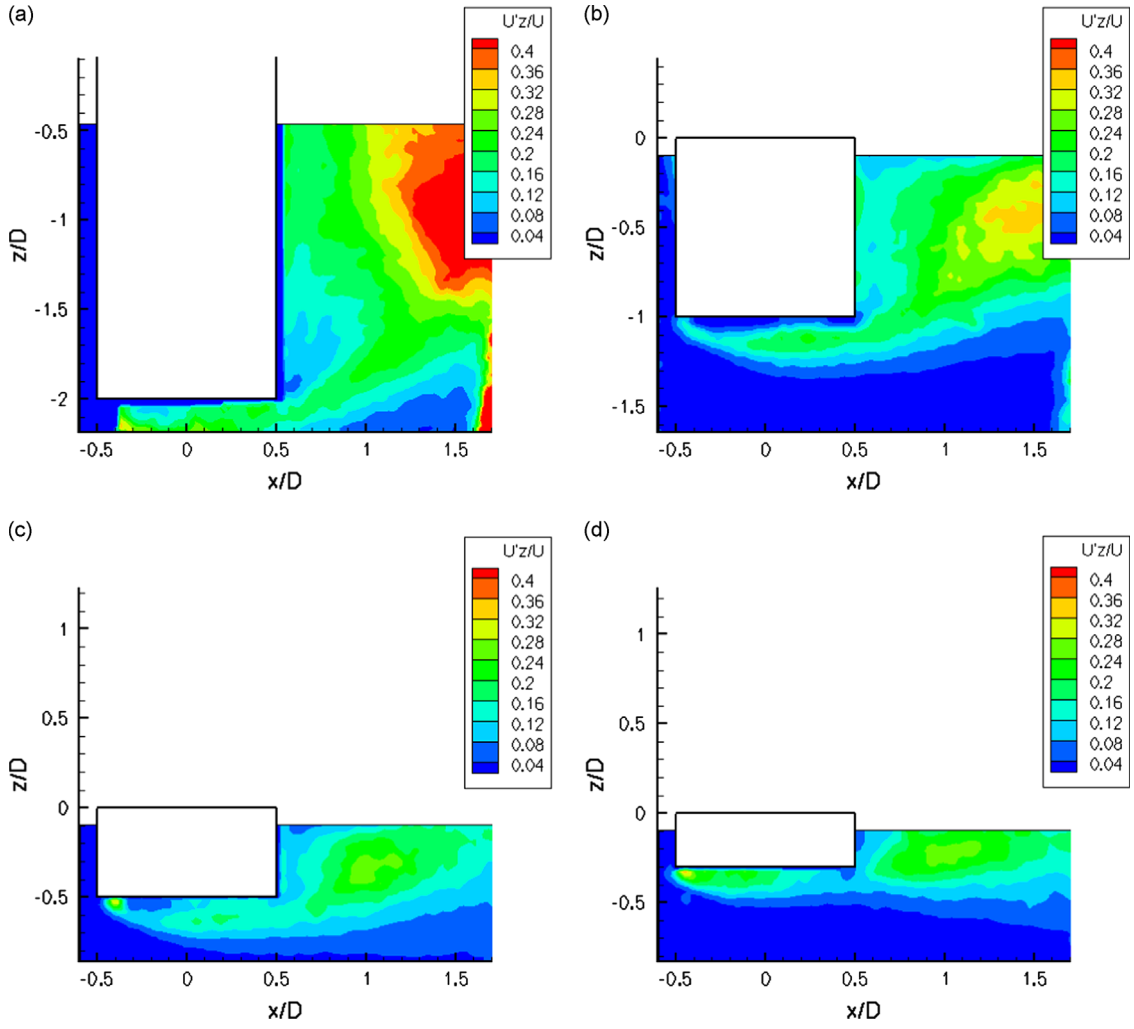

Fig. 21. Contours of root mean square of vertical fluctuations U'_z/U in the vertical center plane at $y/D=0$ for Re=43 000: (a) $L/D=2.0$, (b) $L/D=1.0$, (c) $L/D=0.5$ and (d) $L/D=0.3$.

shear and flapping such that they are the highest in this region. The separation bubble is shorter and distorted for lower aspect ratio cylinders such that the shear layer is weaker and U'_x/U is lower. The origin and behavior of the transversal fluctuations are distinct, as the region of high fluctuations is located around the center plane behind the cylinder. For $L/D=2.0$, the transversal fluctuations are associated with the shedding motion behind the cylinder, and at the border of the separation bubble also by the flapping of the shear layer caused by the shedding; it is the same behavior related by Paulau-Salvador et al. (2010) for $L/D=5.0$ and 2.5. For lower aspect ratio cylinder, $L/D<2.0$ (see Fig. 19(b)–(d)), the shedding is suppressed and the transversal fluctuations are smaller. Von Kármán street characteristics can be verified to diminish for $L/D<2.0$, confirming previous works in the literature.

Figs. 17 and 20 show contours of streamwise, U'_x/U, and transversal, U'_y/U, fluctuations in the horizontal plane near the free end at $z/L=-0.75$ for $L/D=2.0$ and 1.0, respectively. These results show similar behavior compared with lower aspect ratio cylinders. The important in these cases is the distance of the horizontal plane and the cylinder free end. This fact confirms the importance of the effects due to the free-end presence, in which the horizontal fluctuations and the vortex shedding are smaller.

Figs. 18 and 21 show contours of streamwise, U'_x/U, and vertical, U'_z/U, fluctuations in the vertical center plane, respectively. The maximum values of U'_x/U are found in the thin separated shear layer bordering the small recirculation region below the free-end cylinder, as can be seen in Fig. 18. A second region of high values of U'_x/U is found behind the cylinder, but detached from it. This region is not aligned with the shear layer bordering the longitudinal recirculation region, but it is in an orientation similar to the region of high U'_z/U shown in Fig. 21. These results are in agreement with those by Palau-Salvador et al. (2010), which showed a different situation for the longer cylinder case, $L/D=5.0$, as compared with $L/D=2.5$, in which the U'_z/U are not as large and U'_x/U appear to be generated more by shear layer bordering the longitudinal recirculation zone so that the region of high fluctuations is aligned with this.

Our results allow observing that the fluctuation velocities are smaller with decreasing aspect ratio in both measured planes, vertical and horizontal.

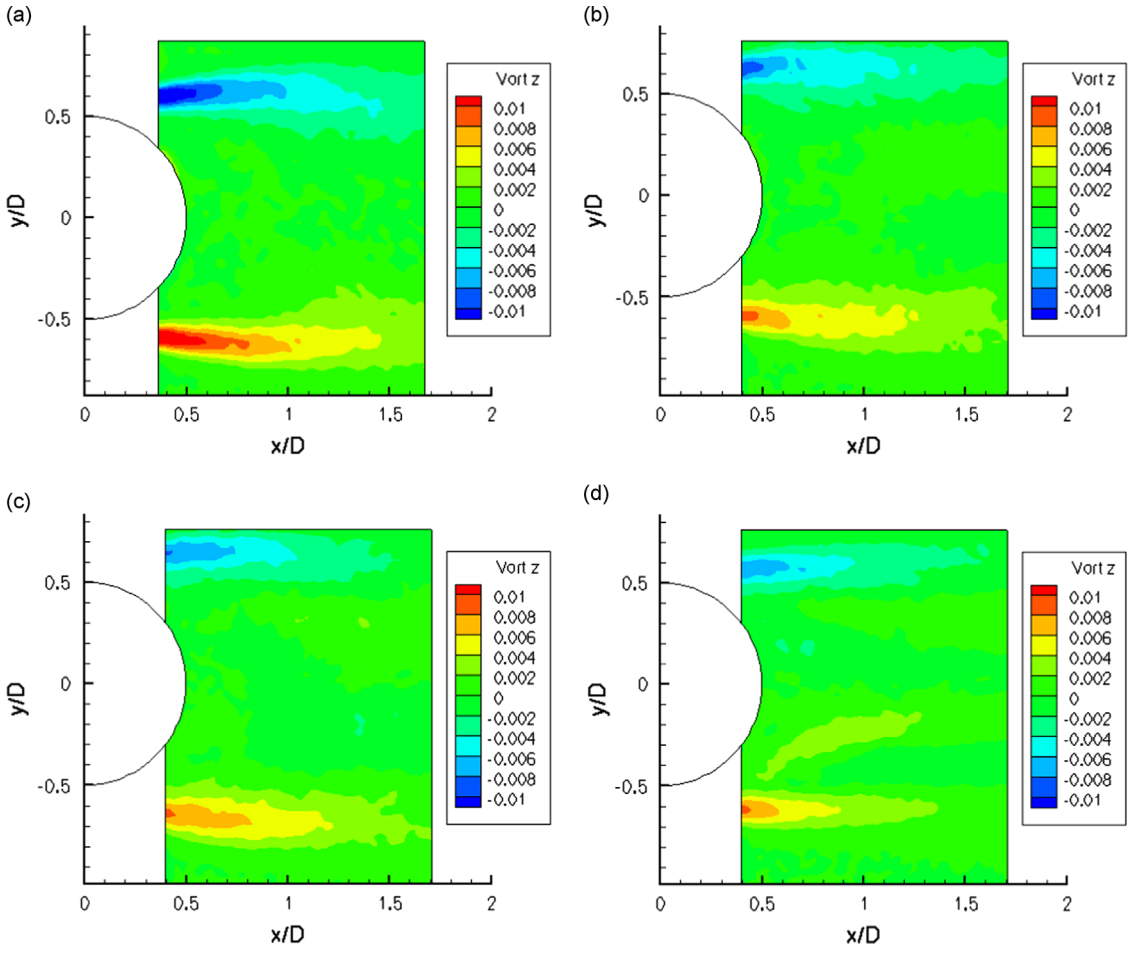

Fig. 22. Contours of mean vertical vorticity $\omega_z D/U$ in the horizontal plane at $z/L=-0.5$ for Re=43 000: (a) $L/D=2.0$, (b) $L/D=1.0$, (c) $L/D=0.5$ and (d) $L/D=0.3$.

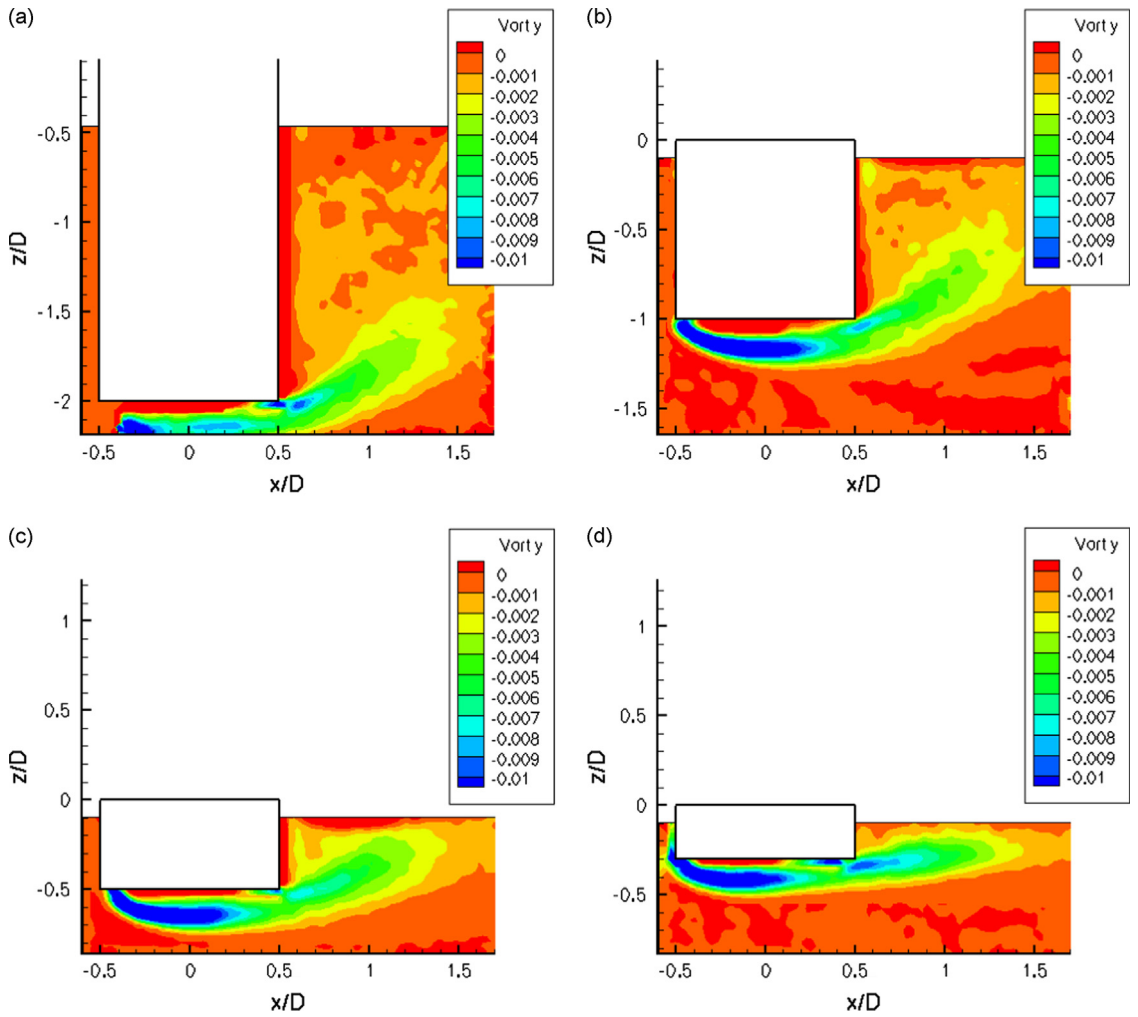

Fig. 23. Contours of mean transverse vorticity $\omega_y D/U$ in the vertical center plane at $y/D=0$ for Re=43 000: (a) $L/D=2.0$, (b) $L/D=1.0$, (c) $L/D=0.5$ and (d) $L/D=0.3$.

Figs. 22 and 23 show contours of mean vertical, $\omega_z D/U$, and transversal, $\omega_y D/U$, vorticity in the horizontal mid-span length plane and vertical center plane, respectively. In general, the flow field in the horizontal plane, as can be seen in Fig. 22, consists of two symmetric vortices with positive or negative values with respect to the wake center plane at $y/D=0$. For $L/D=2.0$ and 1.0, the maximum vorticity peaks occur at $y/D=\pm 0.6$ in the region behind the cylinder; on the other hand, for lower aspect ratio, $L/D=0.5$ and 0.3, the maximum occurs at $y/D=\pm 0.65$. The vertical vorticity, $\omega_z D/U$, decreases with decreasing aspect ratio, which corroborates that the vortex shedding diminishes in the horizontal plane for decreasing aspect ratio. In Park and Lee (2004), the maximum vertical vorticity peaks occur at $y/D=\pm 0.4$ for a cylinder with $L/D=6.0$; moreover, for cylinder with radiussed tip or hemispherical tip, this length increases $y/D=\pm 0.5$ at $|z/L|=0.983$.

Looking at the transverse vorticity, $\omega_y D/U$, in Fig. 23, the shear layer below the free-end cylinder is visible. This remains fairly steady for approximately $0.2D$ below and $0.5D$ behind and above the free end for all aspect ratios. The results showed that for $L/D\leq 0.5$, the entire wake is contaminated with three-dimensional effects due to the free end.

The results for cylinder with very low aspect ratio $L/D\leq 2.0$ showed a distinct behavior for $L/D\leq 1.0$. In these cases, probably the symmetrical vortex shedding is present due to an arch-type vortex formation, as can be seen in the vorticity results in both planes. This result is similar to that obtained by Lee (1997) for aspect ratio below the critical one, and the PIV confirmed these similar structures proposed by the model in Lee (1997).

4. Conclusion

Experiments were carried out in a recirculating water channel regarding the flow around stationary circular cylinders with very low aspect ratio, $0.1\leq L/D\leq 2$, piercing the water free surface.

Force measurements were conducted using a 6dof load cell. The Reynolds number ranged from $10\,000 < \mathrm{Re} < 50\,000$. The forces in the streamwise direction, x, decrease with decreasing aspect ratio, from $\overline{C_x} \sim 1$ for $L/D = 2$ to $\overline{C_x} \sim 0.7$ for $L/D = 0.3$. In the lowest aspect ratio cases, the behavior is different because of the high influence of the forces due to the free-surface effects. The forces in the transverse direction are practically constant, $\overline{C_{y\,rms}} \sim 0.06 \pm 0.01$, for cylinders with $2 \leq L/D \leq 0.75$. The decrease of transverse forces for $L/D < 0.5$ is due to the three-dimensional behavior of the wake in these conditions. The higher three-dimensional behavior of the wake is also responsible for the decrease in the Strouhal number, from $\mathrm{St} \sim 0.15$ for $L/D = 2$ to $\mathrm{St} \sim 0.05$ for $L/D = 0.5$.

The vortex shedding structures can be dominated by a von Kármán street characteristics for $L/D = 2.0$. For $0.75 \leq L/D \leq 1.5$, it can imply that the influence of the structures formed due to the presence of the free end cylinder grows. This behavior affects the transverse force including energy in the same low frequencies as in the streamwise direction. Therefore, the von Kármán street characteristics diminish with decreasing aspect ratio. For $L/D = 0.5$, there is only one dominant frequency that is the same as that in the streamwise direction and it is Re dependent. This frequency is due to the vortex shedding around the cylinder free end. For $L/D = 0.2$, there are not significant energy forces in the transverse direction; in this aspect ratio, the structures formed around the cylinder free end are not able to produce alternating forces. This fact shows $L/D = 0.2$ is a critical value in terms of transverse forces.

PIV measurements were performed for $\mathrm{Re} = 43\,000$. Three different planes were visualized for cylinders with $L/D = 2.0$, 1.0, 0.5 and 0.3. Two horizontal planes namely one mid-span plane at $z/L = -0.5$ and one near the free end at $z/L = -0.75$, and one vertical center plane at $y/D = 0$. The visualizations showed two recirculation regions: the first one over the cylinder free end, and the second one behind the cylinder characterizing a recirculation bubble. These recirculation regions are possibly responsible for forming the arch-type vortex around it; these structures, together with the trailing vortices (with main vorticity streamwise), are mostly responsible for the transverse force around the low aspect ratio, a fact confirmed by the low frequency shedding behavior observed. This model is similar to that presented by Lee (1997), in which arch-type vortex are formed behind the cylinder, and can be the source of the forces in the transverse direction, as can be seen in the case of hemisphere. The fluctuation velocities confirm that there was less regularity of the vortex shedding for $L/D \leq 0.5$. To confirm this conjecture, PIV measurements in the vertical xy plane must be performed.

Acknowledgments

The authors thank Eng. Dr. Ivan Korkischko and Eng. César M. Freire for their help in performing the tests. The authors would also like to acknowledge FAPESP and CAPES for the financial support.

References

Adaramola, M.S., Akinlade, O.G., Sumner, D., Bergstrom, D.J., Schenstead, A.J., 2006. Turbulent wake of a finite circular cylinder of small aspect ratio. Journal of Fluids and Structures 22, 919–928.

Assi, G.R.S., Meneghini, J.R., Aranha, J.A., Coleto, W.G.P., 2005. Design, assembling and verification of a circulating water channel facility for fluid dynamics experiments. *Proceedings of the 18th International Congress of Mechanical Engineering*, COBEM. Ouro Preto, Minas Gerais, Brazil.

Chaplin, J.R., Teigen, P., 2003. Steady flow past a vertical surface-piercing circular cylinder. Journal of Fluids and Structures 18, 271–285.

Cueva, M., Fujarra, A.L.C., Nishimoto, K., Quadrante, L., Costa, A.P., 2006. Vortex-induced motion: model testing of a monocolumn floater. In: Proceedings of the 25th International Conference on Offshore Mechanics and Arctic Engineering, OMAE2006-92167, Hamburg, Germany.

Fox, T.A., WEST, G.S., 1993. Fluid-induced loading of cantilevered circular cylinders in a low-turbulence uniform flow. Part 2: fluctuating loads on a cantilever of aspect ratio 30. Journal of Fluids and Structures 7, 15–28.

Fujarra, A.L.C., Rosetti, G.F., Wilde, J., Gonçalves, R.T., 2012. State-of-art on vortex-induced motion: a comprehensive survey after more than one decade of experimental investigation. In: Proceedings of the 31st International Conference on Ocean, Offshore and Arctic Engineering, OMAE2012-83561, Rio de Janeiro, Brazil.

Gonçalves, R.T., Rosetti, G.F., Fujarra, A.L.C., Nishimoto, K., 2010. Mitigation of vortex-induced motion (VIM) on a monocolumn platform: forces and movements. Journal of Offshore Mechanics and Arctic Engineering 132. (041102-1-16).

Gonçalves, R.T., Rosetti, G.F., Fujarra, A.L.C., Oliveira, A.C., 2012a. Experimental study on vortex-induced motions of a semi-submersible platform with four square columns, Part I: Effects of current incidence angle and hull appendages. Ocean Engineering 54, 150–169.

Gonçalves, R.T., Rosetti, G.F., Fujarra, A.L.C., Franzini, G.R., Freire, C.M., Meneghini, J.R., 2012b. Experimental comparison of two degrees-of-freedom vortex-induced vibration on high and low aspect ratio cylinders with small mass ratio. Journal of Vibration and Acoustics 134, 061009-1–7.

Gonçalves, R.T., Rosetti, G.F., Franzini, G.R., Meneghini, J.R., Fujarra, A.L.C., 2013. Two-degree-of-freedom vortex-induced vibration of circular cylinders with very low aspect ratio and small mass ratio. Journal of Fluids and Structures 39, 237–257.

Govardhan, R.N., Williamson, C.H.K., 1997. Vortex-induced motions of a tethered sphere. Journal of Wind Engineering and Industrial Aerodynamics 69–71, 375–385.

Govardhan, R.N., Williamson, C.H.K., 2005. Vortex-induced vibrations of a sphere. Journal of Fluid Mechanics 531, 11–47.

Griffith, M.D., Leontini, J., Thompson, M.C., Hourigan, K., 2011. Vortex shedding and three-dimensional behavior of flow past a cylinder confined in a channel. Journal of Fluids and Structures 27, 855–860.

Hain, R., Kähler, C.J., Michaelis, D., 2008. Tomographic and time resolved PIV measurements on a finite cylinder mounted on a flat plate. Experiments in Fluids 45, 715–724.

Hay, A.D., 1947. Flow About Semi-submerged Cylinders of Finite Length. Princeton University Report, Princeton, NJ, USA.

Iungo, G.V., Pii, L.M., Buresti, G., 2012. Experimental investigation on the aerodynamic loads and wake flow features of a low aspect-ratio circular cylinder. Journal of Fluids and Structures 28, 279–291.

Kawamura, T., Hiwada, M., Hibino, T., Mabuchi, I., Kumada, M., 1984. Flow around a finite circular cylinder on a flat plate. Bulletin of the Japan Society of Mechanical Engineers 27, 2142–2151.

Khalak, A., Williamson, C.H.K., 1996. Dynamics of a hydroelastic cylinder with very low mass and damping. Journal of Fluids and Structures 10, 455–472.

Korkischko, I., Meneghini, J.R., 2011. Volumetric reconstruction of the mean flow around circular cylinders fitted with strakes. Experiments in Fluids 51, 1109–1122.

Jauvtis, N., Govardhan, R.N., Williamson, C.H.K., 2001. Multiple modes of vortex-induced vibration of a sphere. Journal of Fluids and Structures 15, 555–563.
LEE, L.W., 1997. Wake structure behind a circular cylinder with a free end. Proceedings of the Heat Transfer and Fluid Mechanics Institute, 241–251.
Okamoto, T., Yagita, M., 1973. The experimental investigation on the flow past a circular cylinder of finite length placed normal to the plane surface in a uniform stream. Bulletin of the Japan Society of Mechanical Engineers 16, 805–814.
Palau-Salvador, G., Stoesser, T., Fröhlich, J., Kappler, M., Rodi, W., 2010. Large eddy simulations and experiments of flow around finite-height cylinders. Flow, Turbulence and Combustion 84, 239–275.
Park, C.W., Lee, S., 2000. J. Free end effects on the near wake flow structure behind a finite circular cylinder. Journal of Wind Engineering and Industrial Aerodynamics 88, 231–246.
Park, C.W., Lee, S., 2004. J. Effects of free-end corner shape on flow structure around a finite cylinder. Journal of Fluids and Structures 19, 141–158.
Pattenden, R.J., Turnock, S.R., Zhang, X., 2005. Measurements of the flow over a low-aspect-ratio cylinder mounted on a ground plane. Experiments in Fluids 39, 10–21.
Rahman, M.A.A., Thiagarajan, K., 2013. Vortex-induced vibration of cylindrical structure with different aspect ratio. In: Proceedings of the 17th International Offshore and Polar Engineering Conference. Alaska, USA.
Roddier, D., Finnigan, T., Liapis, S., 2009. Influence of the Reynolds number on spar vortex induced motions (VIM): multiple scale model test comparisons. Proceedings of the 28th International Conference on Ocean Offshore and Arctic Engineering, OMAE2009-79991, Honolulu, HI, USA.
Roh, s.C., Park, S.O., 2003. Vortical flow over the free end surface of a finite circular cylinder mounted on a flat plate. Experiments in Fluids 34, 63–67.
Rosetti, G.F., Vaz, G., Hoekstra, M., Gonçalves, R.T., Fujarra, A.L.C., 2013. CFD calculations for free-surface-piercing low aspect ratio circular cylinder with solution verification and comparison with experiments. *Proceedings of the 32nd International Conference on Ocean, Offshore and Arctic Engineering,* OMAE2013-10963, Nantes, France.
Rostamy, N., Sumner, D., Bergstrom, D.J., Bugg., J.D., 2012. Local flow field of a surface-mounted finite circular cylinder. Journal of Fluids and Structures 34, 105–122.
Sakamoto, H., Arie, M., 1983. Vortex shedding from a rectangular prism and a circular cylinder placed vertically in a turbulent boundary layer. Journal of Fluid Mechanics 126, 147–165.
Savory, T.O.Y., 1986. Hemispheres and hemisphere-cylinders in turbulent boundary layers. Journal of Wind Engineering and Industrial Aerodynamics 23, 345–364.
Schouveiler, L., Provansal, M., 2002. Self-sustained oscillations in the wake of a sphere. Physics of Fluids 14, 3846–3854.
Someya, S., Kuwabara, J., Y., Li, Okamoto, K., 2010. Experimental investigation of a flow-induced oscillating cylinder with two degrees-of-freedom. Nuclear Engineering and Design 240, 4001–4007.
Sumner, D., Heseltine, J.L., Dansereau, O.J.P., 2004. Wake structure of a finite circular cylinder of small aspect ratio. Experiments in Fluids 37, 720–730.
Sumner, D., 2013. Flow above the free end of a surface-mounted finite-height circular cylinder: A review. Journal of Fluids and Structures 43, 41–63.
Tamai, N., Asaeda, T., Tanaka, N., 1987. Vortex structures around a hemispheric hump. Boundary-Layer Meteorology 39, 301–314.
Taniguchi, S., Sakamoto, H., Kiya, M., Arie, M., 1982. Time-averaged aerodynamic forces acting on a hemisphere immersed in a turbulent boundary. Journal of Wind Engineering and Industrial Aerodynamics 9, 257–273.
Van Dijk, R.R.T., Magee, A., Perryman, S., Gebara, J., 2003. Model test experience on vortex induced vibrations of truss spars. In: Proceedings of the Annual Offshore Technology Conference, OTC-15242, Houston, TX, USA.
Waals, O.L., Phadke, A.C., Bultema, S., 2007. Flow induced motions of multi column floaters. In: Proceedings of the 26th International Conference on Offshore Mechanics and Arctic Engineering, OMAE2007-29539, San Diego, CA, USA.
Zhao, M., Cheng, L., 2014. Vortex-induced vibration of a circular cylinder of finite length. Physics of Fluid 26, 015111.